Photocatalytic Decontamination of Airborne T2 Bacteriophage Viruses in a Small-Size TiO2/β-SiC Alveolar Foam LED Reactor

Nizar Doss, Gaëlle Carré, Valérie Keller, Philippe Andre, Nicolas Keller

Photocatalytic decontamination of airborne T2 bacteriophage viruses in a small-size TiO_2/β-SiC alveolar foam LED reactor.

Nizar Doss,[a] Gaëlle Carré,[a,b] Valérie Keller,[a] Philippe André,[b] and Nicolas Keller,[a]*

[a] Institut de Chimie et Procédés pour l'Energie, l'Environnement et la Santé (ICPEES), CNRS, Strasbourg University, 25 rue Becquerel, Strasbourg, France.

[b] Laboratoire de Biophotonique et Pharmacologie, CNRS and Strasbourg University, 74 route du Rhin, Illkirch, France.

* nkeller@unistra.fr - Nicolas Keller - Fax: +33(0)368852761; Tel: +33(0)368852811

KEYWORDS. LED; Photocatalysis; Titanium dioxide; T2 bacteriophage virus; Solid alveolar foams; Energy effectiveness

ABSTRACT

Light emitting diodes (LEDs) emitting at 392 nm were successfully used as an irradiation light source and associated to TiO_2/β-SiC solid alveolar foams for designing a small-size, flow-through structured photocatalytic device for purifying air from airborne T2 bacteriophage viruses. Light emitting diodes are characterized by a high electricity-to-light yield, strength, a long lifetime, to ability to use a direct current power source, an almost-complete recycling rate, and a lack of mercury.

Irrespective of the number of LEDs, we showed that the decontamination efficiency associated with removing airborne T2 bacteriophage viruses resulted from both the photocatalytic activity and the passive filtration effect of the TiO_2/β-SiC solid alveolar foams. A high photocatalytic filtration efficiency was observed with 56 LEDs and a logarithmic abatement of 3 was achieved for 60 min of run time, with an apparent time constant of 11.0 min after correcting for the natural decay of the bioaerosol. The pure filtration effect corresponded to a logarithmic abatement of 1, with an apparent time constant of 43.1 min. The interest in using 56 LEDs *vs.* 40 LEDs was highlighted in terms of the logarithmic abatement as well as energy effectiveness.

1. Introduction

Indoor air quality control is garnering growing interest due to public concerns over human health. The United States Environmental Protection Agency (EPA) considers indoor air pollution to be one of the primary environmental risks to public health given that humans spend roughly 80% of their time indoors (*i.e.*, in confined places) where pollutant concentrations are higher (EPA 1997). Malodorous, toxic or global warming-related chemical pollutants have been the most studied targets, but the removal of airborne microorganisms is also a challenging field. Indeed, the continuously growing resistance of microorganisms to chemical treatments and their dissemination due to the intensification of transport mechanisms are responsible for threats associated with biological pollutants. Although many airborne microorganisms are not virulent or only minimally so, it is well known that many kinds of airborne microorganisms such as bacteria, viruses and fungi are considered to be hazardous to human health. These airborne microorganisms have a pronounced societal impact in terms of costs and mortality (WHO 2007).

The removal of chemical or airborne biological pollutants is therefore a challenging task. Oxidative photocatalysis has attracted attention in recent decades as an efficient air treatment technology because of the strong oxidizing power of UV-A-irradiated semiconductors at room temperature (Herrmann 1999; Ohtani 2010; Ollis et al. 2010). The organic nature of microorganism constituents has resulted in the establishment of a meaningful analogy between biological and chemical targets: indeed, *e.g.*, cell walls are viewed as a complex assembly of high molecular-weight organic compounds that photocatalysis can oxidize *via* oxidative photoholes or hydroxyl radicals. Therefore, irradiated photocatalysts cause oxidative damages to cell membranes, which are considered to be the first barrier to maintaining vital cell functions. As a result of this process, inactivation of bacteria, viruses, spores and yeasts can be achieved (Matsunaga et al. 1985; Blake et al. 1999; Gogniat et al. 2006; Josset et al. 2008; Herrmann 2010; Nakata and Fujishima 2012).

While photocatalysis has been already widely applied for removing chemical pollutants in environmental remediation efforts in water, air as well as on surfaces, the application of photocatalysis

to biological objects mainly concerns the disinfection of water and the implementation of self-decontaminating coatings (Blake et al. 1999). The photocatalytic disinfection of contaminated air (*i.e.*, bioaerosols) has been rarely investigated despite a large range of applications and pronounced public health concerns. This situation largely stems from the difficulty of working with bioaerosols. However, studies with bioaerosols have focused on a wide range of microorganisms such as *Escherichia coli*, *Legionella pneumophila*, *Microbacterium sp.*, *Bacillus subtilis*, *Bacillus cereus*, *Staphylococcus aureus*, *Aspergillus brasiliensis*, a Candida famata yeast, and MS2 and λ phage viruses (Goswami et al. 1997; Keller et al. 2005; Vohra et al. 2006; Grinshpun et al. 2007; Josset et al. 2007, 2010; Pal et al. 2008; Yu et al. 2008).

Therefore, the development of three-dimensional photocatalytic media such as alveolar solid foams that could take advantage of the simultaneous filtration and photocatalytic removal of airborne microorganisms is of interest. These media benefit from a static mixer role and a very low pressure drop, and they enable suitable light transmission to the reactor core. For these reasons, they are worth studying for designing flow-through structured reactors (Kato et al. 2005; Ochuma et al. 2007; Yuan et al. 2008; Yao et al. 2011; Ochiai and Fujishima 2012; Ishiguro et al. 2013; Masson et al. 2015). In the field of light sources, high-output, inexpensive light emitting diodes (LEDs) have garnered strong interest as a promising photochemical light source for replacing widespread traditional fluorescent lamps in environmental remediation applications (Wang and Ku 2006; Chen et al. 2007; Shie et al. 2008; Lapkin et al. 2008; Gosh et al. 2008, 2009; Liu et al. 2009; Subagio et al. 2011; Doss et al. 2014). Indeed, the advantages exhibited by LEDs relate to their high electricity-to-light yield with minimal heating, their low energy consumption and a more sustainable Hg-free nature. Nearly complete recycling of LEDs is possible, and they benefit from a long lifetime and a small size that enables system miniaturization and configuration flexibility.

Ultraviolet and visible-light LEDs have been already successfully implemented in gas- and liquid-phase photocatalytic reactors for the degradation of model molecules such as Reactive Red 22 and *o*-cresol (Wang and Ku 2006; Chen et al. 2007), 4-chlorophenol (Gosh et al. 2008, 2009), orange methyl (Liu et al. 2009), bisphenol-A in water (Subagio et al. 2011), and formaldehyde (Shie et al.

2008) and methyl ethyl ketone (Doss et al. 2014) in air. Due to cost limitations in the case of high-irradiance UV-A LEDs, studies have been mainly performed using more intense and cheaper visible LEDs.

Our previous investigations of airborne microorganisms were concerned with the UV-A photocatalytic treatment of flowing air contaminated by *L. pneumophila*, *Escherichia coli*, T2 bacteriophage viruses and *B. atrophaeus* using conventional fluorescent UV-A lamps and a classical reactor geometry (Keller et al. 2005; Josset et al. 2007, 2010). We previously notably highlighted the importance of the aerodynamics in air decontamination, directly resulting from the microorganism morphology, so that the results obtained from studies performed toward chemical pollutants, cannot be simply transposed to airborne microorganisms. Therefore, the aim of this paper was to report the first use of a flow-through LED photocatalytic reactor structured by open-cell β-SiC alveolar foams for decontaminating air from airborne T2 bacteriophage viruses. β-SiC alveolar foams are open cellular structures benefiting from a static mixer role, from very low pressure drops and from an increased surface-to-reactor volume ratio while maintaining a suitable light transmission to the reactor core, so that they are good candidates for elaborating flow-through photoreactors (Keller et al. 20013; Doss et al. 2014; Masson et al. 2015). In addition, their β-SiC nature provides a strong chemical and thermal stability to the material, allowing chemical/thermal regeneration treatments to be applied if necessary. Here, we therefore demonstrated the ability of the foam-structured LED reactor to decontaminate flowing air, which resulted from a combined photocatalytic and filtration effect.

2. Experimental Section

2.1. Material preparation

The TiO_2 MPT623 material was supplied by Ishihara Sangyo Kaisha. TiO_2 MPT623 is a visible light-responsive Pt chloride-modified rutile TiO_2 photocatalyst that has been already used for practical indoor air remediation applications (Yu et al. 2010; Nishikawa et al. 2012).

Medium surface area, open-cell β-SiC alveolar foam was synthesized by the SICAT Company (Willstätt-Germany) according to the Shape Memory Synthesis (SMS) replica method. In this method,

a pre-shaped polyurethane foam is transformed into its corresponding carbide at 1360°C in an argon atmosphere (Nguyen and Pham 2011). This SMS replica synthesis reflects the fact that the original macrostructural features of the pre-shaped polyurethane foam were retained after synthesis. Therefore, the β-SiC solid foams can be manufactured with different shapes to conform to a particular photoreactor's geometry. These foams were modeled by Edouard and colleagues (Huu et al. 2009) as the packing of regular pentagonal dodecahedrons. The most characteristic parameters of the β-SiC foam are considered to be their cell size (ϕ),pore or window diameter (a)—which correlates with the pore density (*i.e.*, the number of pores per linear inch, ppi)—and the strut diameter (ds).

The deposition of the TiO_2 MPT623 photocatalyst onto the alveolar β-SiC foam was performed by plunging the β-SiC foam support in a TiO_2-containing water suspension and then drying the sample at ambient temperature. The impregnation suspension, with a TiO_2 concentration of 100 g/L, was stirred for 30 min before the foam was plunged. The impregnation process was replicated, with a pressurized air flow treatment between each step, until the desired TiO_2 mass was obtained. The TiO_2 wt.% content was determined by weighting the β-SiC foam-coated TiO_2 material after a final drying at 100°C and subsequent ultrasonic treatment.

2.2. Characterization techniques

X-ray diffraction (XRD) measurements were carried out on a D8 Advance Bruker diffractometer in θ/θ mode with $K\alpha_1$ radiation of Cu at 1.5406 Å.

Surface area measurements were carried using a Micrometrics Tristar 3000 with N_2 as an adsorbant at -196°C. The samples had been previously outgassed at 200°C for 8 h to desorb impurities or moisture. The BET-specific surface area was calculated from the N_2 adsorption isotherms, and the micropore surface area was derived using the *t*-plot method.

Scanning electron microscopy (SEM) was carried out in secondary electron mode on a JEOL-JSM-6700 F microscope equipped with a field emission gun, and operated with an extraction potential ranging from 1–10 kV. Prior to the analysis, the samples were coated with gold.

UV-visible absorption spectra of the materials were recorded on a Varian Cary 100 Scan spectrophotometer equipped with a DRA-CA-301 *Labsphere* diffuse reflectance cell.

UV-A irradiance measurements were performed using a wideband RPS900-W Rapid Portable Spectroradiometer from International Light Technologies (Peabody, MA, USA). The measurements were performed as close as possible to a single LED. The UV-A irradiance values suffered from a non-negligible uncertainty because of difficulties recording the irradiance close to the LED surface; the LED geometry required averaging the data recorded for different locations on the LED surface.

The light transmission through the β-SiC foam was defined as the fraction of the incident light, in terms of UV-A irradiance, transmitted through the material as the foam thickness was varied.

2.3. LED light sources and photocatalytic reactors

The LEDs (ref. VL390-5-15) were purchased from Roithner Lasertechnik (Austria). These InGaN-based LEDs had a viewing angle of 15° (technical data provided by the supplier).

A photocatalytic reactor was engineered to incorporate 40 or 56 LEDs and a 65 *x* 40 mm (*d x h*) disk-shaped TiO_2/β-SiC foam photocatalyst with a mean cell cell size of 5440 µm (Fig. 1). The photocatalytic reactor also included an inner fan functioning at 10 m^3/h and the printed circuit boards for LEDs. The TiO_2/β-SiC foam photocatalyst disk occupied a total volume of 133 mL, so that the tests were performed with a residence time of 0.048 s.

2.4. T2 bacteriophage preparation and photocatalytic test procedure

The recirculation tests were operated at an airflow rate of 10 m^3/h in a 0.8-m^3 glovebox adapted for airborne microorganisms that acted as a reaction chamber. The test chamber was homogenized via the use of an additional fan operating at a higher airflow rate (30 m^3/h).

We used nanometer-size T2 bacteriophage viruses as model viruses for airborne viruses. Bacteriophages are viruses that infect specific bacteria, and T2 bacteriophages evolute on an *E. coli* host bacteria (strain: BAM). To obtain the bacteriophage suspension, an aliquot of a -80°C high titre stock of T2 bacteriophages (roughly 10^{10} T2/mL) was first diluted to the tenth using a sterile $MgSO_4$ solution (10 mM), and subsequently till a dilution factor of 10^8 (4 replicates for each dilution). 0.1 ml of each dilution of bacteriophages was poured onto a Luria Bertani (LB) agar plate and a soft LB agar (0.75% LB agar) containing the *E. coli* host strain was prepared simultaneously using the following

methodology. One aliquot (100 μL) of the *E. coli* BAM suspension in an exponential growth phase was diluted in physiological water to an optical density of 0.5 at 600 nm and was mixed with 50 mL of soft LB agar in surfusion (50°C). 5 mL of this mix was sprayed onto previously prepared LB agar plates. The plates were incubated at 37°C for 24 h. Viral infection resulted in clear zones (or plaque) due to lysis by bacteriophages, and zones where bacterial growth occurred were turbid. After 24 h of incubation at 37°C, 5 mL of a sterile $MgSO_4$ solution (10 mM) was poured on the surface of the plates with 1000–5000 lysis plaques. These plates were left an agitating plate at 4°C for 2 h, which allowed the viruses to diffuse into the liquid phase free of bacterial debris. The supernatants were collected, and chloroform was added to lyse the bacterial cells and liberate the phages within to a final concentration of 0.2% v/v. This stock suspension was stored at 4°C was then titrated following a standard lysis plaque procedure.

The contaminated bioaerosol was obtained by aerosolizing a 5 mL aliquot of a 6×10^6 T2 bacteriophages/mL suspension into the reaction chamber as droplets in a high-flow rate air stream (3.8×10^7 bacteriophages per m^3 of air). At the reactor outlet, T2 bacteriophages impacted the surface of the LB agar plates for 1 min at 10-min time intervals. Then, the surface was recovered with 5 mL of soft LB agar in surfusion (50°C) mixed with 100 µL of a *E. coli* BAM suspension in an exponential growth phase, which had been previously diluted in LB to an optical density of 0.5 at 600 nm. The plates were then incubated for 24 h at 37°C prior to the numeration of lysis plaques.

3. Results and Discussion

3.1. Material characterization

The XRD pattern of TiO_2 MPT623 shown in Figure 2A exhibits diffraction peaks corresponding to rutile TiO_2, with main peaks at 27.5°, 36.1° and 54.4° corresponding to the (110), (101) and (211) planes, respectively (Dai et al. 2010). TiO_2 MPT623 has a non-microporous specific surface area of 60 m^2/g. Figure 2B shows the LED emission spectral range compared with the absorption range of TiO_2 MPT623. The LEDs have been labeled here as LED-392 according to their measured wavelength of emission maximum at 392 nm. The total measured irradiance is 11.7 ± 2.0 mW/cm^2 with a spectral

bandwidth of 15 nm. Those LEDs are considered to be UV-Vis LEDs, and they allow an activation of the rutile TiO_2 photocatalyst in the UV-A range and in the beginning of the visible light region. Indeed, rutile TiO_2 is reported to have a band gap of 3.0 eV and a band edge at 413 nm (Kavan et al. 1996; Bosc et al. 2007), whereas the LEDs had a spectral bandwidth of 15 nm and a maximum emission wavelength of 392 nm.

The optical and SEM images in Figure 3A show the macroscopic features of the open-cell TiO_2/β-SiC foam catalyst and the uniformity of the TiO_2 coating. The parameters of the solid β-SiC alveolar foam were measured using optical imaging to be 5440 ± 720 µm, 2290 ± 630 µm and 575 ± 80 µm in terms of cell size, window size and strut diameter, respectively. These parameters are as defined in the model developed by Edouard (Huu et al. 2009), with a 95–97% open porosity. Figure 3B shows the light transmission through the β-SiC foam as a function of foam thickness, with a light transmission following a $T_t = e^{-t/\lambda}$ first-order decreasing exponential model as a function of the foam thickness *t*, with λ = 0.47 ± 0.02 cm representing the characteristic length for the β-SiC foam. We selected a β-SiC foam thickness of 0.4 cm to ensure auitable light penetration to the core of the foam.

The β-SiC foam used as a structured support had a specific surface area of 20 m^2/g; after the impregnation process the resulting TiO_2/β-SiC foam catalyst had a TiO_2 content of 9.2 ± 0.2 wt.% corresponding to 1.6 g of TiO_2 within the reactor, and exhibited a specific surface area of 24 m^2/g.

3.2. Decontamination efficiency

Figure 4 shows the decontamination kinetics of the T2 phage virus bioaerosol obtained with the 40- and 56-LED TiO_2/β-SiC foam-structured photocatalytic reactors, expressed as the evolution with time of both the contamination and the logarithmic abatement. The decontamination kinetics resulting from a pure filtration effect were reported, as well as the blank test results, which represent the stability of the bioaerosol within the test chamber as a function of time.

The degradation of chemicals is typically expressed following the Langmuir-Hinshelwood model for deriving the apparent kinetic rate constant in an apparent first-order reaction for highly diluted samples (Cunningham et al. 1994; Minero et al. 2013). Similarly, we used an apparent first-order

decontamination kinetic for the T2 virus bioaerosol. We adopted an apparent time constant (τ) to characterize the decontamination performance (Eq. 1):

$$\%C(t) = 100\% \times e^{-t/\tau} \quad (1)$$

where %*C(t)* is the contamination of the test chamber as a percent.

The evolution of the contamination with time within the test chamber during blank tests was characterized by defining τ^{b}, the apparent time constant. The $\tau^{filtration}$ apparent time constant was derived from the tests using the non-irradiated TiO_2/β-SiC foam-structured reactor irrespective of the number of LEDs. This constant has to be corrected from the natural decay of the bioaerosol for not determining the abatement resulting only from a filtration effect. We accordingly obtained the corrected $\tau^{filtration}_{corr}$ apparent time constant (Eq. 4). Similarly, the τ^{photo} apparent time constant was derived from the photocatalytic tests and had to be corrected from the natural decay of the bioaerosol for determining the abatement resulting only from the photocatalytic filtration effect. We consequently obtained the corrected τ^{photo}_{corr} apparent time constant (Eq. 5). Therefore, we can derive the following data:

$$\%C_{corr}^{filtration}(t) = 100\% \times \left(e^{-t/\tau_{corr}^{filtration}}\right) = \frac{\%C^{filtration}(t)}{\%C^{b}(t)} = \frac{100\% \times e^{-t/\tau filtration}}{100\% \times e^{-t/\tau^{b}}} = 100\% \times \left(e^{-t/\tau filtration} + e^{t/\tau^{b}}\right) \quad (2)$$

$$\%C_{corr}^{photo}(t) = 100\% \times \left(e^{-t/\tau_{corr}^{photo}}\right) = \frac{\%C^{photo}(t)}{\%C^{b}(t)} = \frac{100\% \times e^{-t/\tau photo}}{100\% \times e^{-t/\tau^{b}}} = 100\% \times \left(e^{-t/\tau photo} + e^{t/\tau^{b}}\right) \quad (3)$$

The corrected apparent time constants were derived as follows:

$$\tau_{corr}^{filtration} = \frac{\tau^{b} \times \tau^{filtration}}{\tau^{b} - \tau^{filtration}} \quad (4)$$

$$\tau_{corr}^{photo} = \frac{\tau^{b} \times \tau^{photo}}{\tau^{b} - \tau^{photo}} \quad (5)$$

The energy effectiveness (E_e) was calculated from Eq. 6 for the removal of T2 airborne viruses, as adapted from the works of Shie and Pai (2010) on the degradation of Volatile Organic Compounds, as follows:

$$Energy\ effectiveness\ (E_e, log.kW^{-1}h^{-1}) = \frac{T2\ virus\ logarithmic\ abatement}{input\ power\ (kW.h)} = \frac{log}{p \times t \times V} \quad (6)$$

where V is the chamber volume (L), p is the consumed energy power (kW) and t is the reaction time (h).

Table 1 reports the decontamination results obtained with 40- and 56-LED TiO_2/β-SiC foam-structured photocatalytic reactors in terms of the apparent time constant, and the energy effectiveness coefficients of the different systems (calculated for 60 min of run time), which corresponded to the duration of use necessary to attain a logarithmic abatement of 3 with the most efficient system (*i.e.*, the photocatalytic filtration with 56 LEDs).

It is worth noting that a natural decay was observed during the blank tests, which resulted from (i) the possible instability of the bioaerosols during the test and (ii) the high recirculation flow rate used, which led to some microorganisms impacting the chamber walls. Therefore, natural decay during the blank tests was characterized with an apparent time constant of 52.1 min. It is worth noting that the non-irradiated TiO_2/β-SiC foam-structured reactor—irrespective of the number of LEDs—displayed a pure filtration efficiency characterized by a logarithmic abatement of 1. The reactor was characterized by an apparent time constant of 23.6 min before correction and an apparent time constant of 43.1 min after correcting for bioaerosol stability.

A logarithmic abatement of 1.75 was achieved after 60 min with the system with 40 LEDs, with an apparent time constant of 20.5 min before correction and an apparent time constant of 33.8 min after correction. This finding revealed the contribution of the photocatalytic activity of foams in addition to their filtration efficiency obtained with 40 LEDs. On the other hand, a higher photocatalytic filtration efficiency with a logarithmic abatement of 3 was achieved after 60 min of run

time using the TiO_2/β-SiC foam-structured reactor irradiated by 56 LEDs with an apparent time constant of 9.1 min before correction and an apparent time constant of 11.0 min after correction.

These results highlighted the utility of using large cell-size foams for structuring reactors to take advantage of a large cell size for providing illumination to the core of the reactor while still enabling a decontamination efficiency based on the pure filtration effect within the alveolar foam. As a result, the global airborne microorganism abatement directly resulted from both photocatalytic activity and passive filtration.

After correcting for bioaerosol stability and despite an increased energy need, increasing the number of LEDs from 40 to 56 was beneficial in terms of the energy effectiveness coefficient. Indeed, the foam-structured reactor with 56 LEDs exhibited an energy effectiveness of 5.5 x 10^{3} $log.kW^{-1}h^{-1}$ *vs*. 4.5 x 10^{3} $log.kW^{-1}h^{-1}$ for a similar system with 40 LEDs. After correcting for the bioaerosol stability within the chamber, the energy effectiveness was boosted to 4.6 x 10^{3} $log.kW^{-1}h^{-1}$ using 56 LEDs *vs*. 3.2 x 10^{3} $log.kW^{-1}h^{-1}$ for the set-up with 40 LEDs. Therefore, the increase in the energy need associated with increasing the number of LEDs was largely overcome by the pronounced increase in the logarithmic abatement.

4. Conclusion

A small-size flow-through photocatalytic device incorporating a medium surface area, large-cell size β-SiC alveolar foam as a structured photocatalyst support and LEDs as an irradiation light source has been engineered to develop an air-purifying technology that is efficient at decontaminating airborne T2 bacteriophage viruses. Using TiO_2 MPT623 as a photocatalyst, a system incorporating 56 LEDs emitting at 392 nm exhibited a high photocatalytic filtration activity, with a logarithmic abatement of 3 for 60 min of run time, for which a 10-fold abatement resulted from the passive filtration effect of the alveolar foam.

Irrespective of the number of LEDs, the decontamination effect resulted from both the photocatalytic activity and the passive filtration effect of the TiO_2/β-SiC solid alveolar foams. The

utility of using 56 LEDs *vs.* 40 LEDs was highlighted in terms of the logarithmic abatement as well as the energy effectiveness. Our results have illuminated interest in using a supporting solid alveolar foam and small-size LEDs as a valuable alternative for searching for efficient and energy-saving technologies.

Acknowledgments

The authors are grateful to DGA (Direction Générale de l'Armement) and Alsace regional council for financially supporting this work in the frame of the PhD grant of G. Carré. Prof. M.-C. Lett is deeply thanked for her participation to this study. Drs. C. Pham and P. Nguyen from SICAT Catalyst are thanked for providing β-SiC alveolar foams.

Literature

Blake, D.M., Maness, P. C., Huang, Z., Wolfrum, E.J., Huang, J., Jacoby, W.A. (1999) Application of the photocatalytic chemistry of titanium dioxide to disinfection and the killing of cancer cells. Separation and Purification Methods, 28, 1-50.

EPA (1997). Exposure factors handbook. US Environment protection agency, Washington, DC., Ch. 15:Table 15-176.

Bosc, F., Ayral, A., Keller, N., Keller, V. (2007) Room temperature visible light oxidation of CO by high surface area rutile TiO_2-supported metal photocatalyst. Applied Catalysis B: Environmental, 69, 133-137.

Chen, H.W., Ku, Y., Irawan, A. (2007) Photodecomposition of o-cresol by UV-LED/TiO_2 process with controlled periodic illumination. Chemosphere, 69, 184-190.

Cunningham, J., Al-Sayyed, G., Srijaranai, S. (1994) Adsorption of model pollutants onto TiO_2, particles in relation to photoremediation of contaminated water, In G.R. Helz, R.G. Zepp & D.G. Crosby (Eds), Aquatic and Surface Photochemistry (pp. 317-348), Boca Raton (FL): Lewis.

Dai, S., Wu, Y., Sakai, T., Du, Z., Sakai, H., Abe, M. (2010) Preparation of Highly Crystalline TiO_2 Nanostructures by Acid-assisted Hydrothermal Treatment of Hexagonal-structured Nanocrystalline

Titania/Cetyltrimethyammonium Bromide Nanoskeleton. Nanoscale Research Letters, 5, 1829-1835.

Doss, N., Bernhardt, P., Romero, T., Masson, R., Keller, V., Keller, N. (2014) Photocatalytic degradation of butanone (methylethylketone) in a small-size TiO_2/β-SiC alveolar foam LED reactor. Applied Catalysis B: Environmental, 154–155, 301-308.

Gogniat, G., Thyssen, M., Denis, M., Pulgarin, C., Dukan, S. (2006) The bactericidal effect of TiO_2 photocatalysis involves adsorption onto catalyst and the loss of membrane integrity. FEMS Microbiology Letters, 258(1), 18-24.

Ghosh, J.P., Langford, C.H., Achari, G. (2008) Characterization of an LED Based Photoreactor to Degrade 4-Chlorophenol in an Aqueous Medium Using Coumarin (C-343) Sensitized TiO_2. The Journal of Physical Chemistry A, 112, 10310-10314.

Ghosh, J.P., Sui, R., Langford, C.H., Achari, G., Berlinguette, C.P. (2009) A comparison of several nanoscale photocatalysts in the degradation of a common pollutant using LEDs and conventional UV light. Water Research, 43, 4499-4506.

Goswami, D.Y., Trivedi, D.M., Block, S.S. (1997) Photocatalytic disinfection of indoor air. Journal of Solar Energy Engineering, 119, 92-96.

Grinshpun, S.A., Adhikari, A., Honda, T., Kim, K.Y., Toivola, M., Rao, K.S.R., Reponen, T. (2007) Control of aerosol contaminants in indoor air: Combining the particle concentration reduction with microbial inactivation. Environmental Science & Technology, 41, 606-612.

Herrmann, J.-M. (1999) Heterogeneous photocatalysis: fundamentals and applications to the removal of various types of aqueous pollutants. Catalysis Today 53(1), 115-129.

Herrmann, J.-M. (2010) Fundamentals and misconceptions in photocatalysis. Journal of Photochemistry and Photobiology A: Chemistry, 216(2-3), 85-93.

Huu, T.T., Lacroix, M., Pham Huu, C., Schweich, D., Edouard, D. (2009) Towards a more realistic modeling of solid foam: Use of the pentagonal dodecahedron geometry. Chemical Engineering Science 64(24), 5131-5142.

Ishiguro, H., Yao, Y., Nakano, R., Hara, M., Sunada, K., Hashimoto, K., Kajioka, J., Fujishima, A., Kubota, Y. (2013) Photocatalytic activity of Cu^{2+}/TiO_2-coated cordierite foam inactivates bacteriophages and *Legionella pneumophila*. Applied Catalysis B: Environmental, 129, 56-61.

Josset, S., Hajiesmaili, S., Begin, D., Edouard, D., Pham-Huu, C., Lett, M.C., Keller, N., Keller, V. (2010) UV-A photocatalytic treatment of *Legionella pneumophila* bacteria contaminated airflows through three-dimensional solid foam structured photocatalytic reactors. Journal of Hazardous Materials 175(1-3), 372-381.

Josset, S., Keller, N., Lett, M.-C., Ledoux, M.J., Keller, V. (2008) Numeration methods for targeting photoactive materials in the UV-A photocatalytic removal of microorganisms. Chemical Society Reviews, 37, 744-755.

Josset, S., Taranto, J., Keller, N., Keller, V., Lett, M.-C., Bonnet, V. (2007) UV-A photocatalytic treatment of high flow rate air contaminated with *Legionella pneumophila*. Catalysis Today, 129, 215-222.

Kato, S., Hirano, Y., Iwata, M., Sano, T., Takeuchi, K., Matsuzawa, S. (2005) Photocatalytic degradation of gaseous sulfur compounds by silver-deposited titanium dioxide. Applied Catalysis B: Environmental, 57(2),109-115.

Kavan, L., Grätzel, M., Gilbert, S.E., Klemenz, C., Scheel, H.J. (1996) Electrochemical and Photoelectrochemical Investigation of Single-Crystal Anatase. The Journal of American Chemical Society, 118(28), 6716-6723.

Keller, N. ; Robert, V. ; Keller, V. (2013) Immobilization of a semiconductor photocatalyst on solid supports: methods, materials and applications, in: P. Pichat (Ed.), Photocatalysis and Water Purification: From Fundamentals to Recent Applications (pp. 145-178), Weinheim: Wiley-VCH.

Keller, V., Keller, N., Ledoux, M.J., Lett, M.-C. (2005) Biological agent inactivation in a flowing air stream by photocatalysis. Chemical Communications, 2918-2920.

Lapkin, A.A., Boddu, V.M., Aliev, G.N., Goller, B., Polisski, S., Kovalev, D. (2008) Photo-oxidation by singlet oxygen generated on nanoporous silicon in a LED-powered reactor. Chemical Engineering Journal, 136(2-3), 331-336.

Liu, Y., Liu, J., Lin, Y., Zhang, Y., Wei, Y. (2009) Simple fabrication and photocatalytic activity of S-doped TiO_2 under low power LED visible light irradiation. Ceramics International, 35, 3061-3065.

Masson, R., Keller, V., Keller, N. (2015) β-SiC alveolar foams as a structured photocatalytic support for the gas phase photocatalytic degradation of methylethylketone. Applied Catalysis B: Environmental, 170-171, 301-311.

Matsunaga, T., Tomoda, R., Nakajima, T., Wake, H. (2008) Photoelectrochemical sterilization of microbial cells by semiconductor powders. FEMS Microbiology Letters, 29, 211-214.

Minero, C., Maurino, V., Vione, D. (2013) Photocatalytic Mechanisms and Reaction Pathways Drawn from Kinetic and Probe Molecules. In P. Pichat (Ed.), Photocatalysis and water purification : From Fundamentals to Recent Applications (pp. 53-72). Weinheim: Wiley-VCH.

Nakata, K. & Fujishima, A. (2012) TiO_2 photocatalysis: Design and applications. Journal of Photochemistry and Photobiology C: Photochemistry Reviews, 13(3), 169-189.

Nguyen, P. & Pham, C. (2011) Innovative porous SiC-based materials: From nanoscopic understandings to tunable carriers serving catalytic needs. Applied Catalysis A: General, 391(1-2), 443-454.

Nishikawa, M., Sakamoto, H., Nosaka, Y. (2012) Reinvestigation of the Photocatalytic Reaction Mechanism for Pt-Complex-Modified TiO_2 under Visible Light Irradiation by Means of ESR Spectroscopy and Chemiluminescence Photometry. The Journal of Physical Chemistry A, 116, 9674-9679.

Ochiai, T. & Fujushima, A. (2012) Photoelectrochemical properties of TiO_2 photocatalyst and its applications for environmental purification. Journal of Photochemistry and Photobiology C: Photochemistry Reviews, 13(4), 247-262.

Ochuma, I.J., Osibo, O.O., Fishwick, R.P. Pollington, S., Wagland, A., Wood, J., Winterbottom, J.M. (2007) Three-phase photocatalysis using suspended titania and titania supported on a reticulated foam monolith for water purification. Catalysis Today,128, 100-107.

Ohtani, B. (2010) Photocatalysis A to Z—What we know and what we do not know in a scientific sense. Journal of Photochemistry and Photobiology C: Photochemistry Reviews 11(4), 157-178

Ollis, D.F., Pichat, P., Serpone, N. (2010) TiO_2 photocatalysis-25 years. Applied Catalysis B: Environmental, 99(3-4), 377.

Pal, A., Pehkonen, S.O., Yu, L.E., Ray, M.B. (2008) Photocatalytic Inactivation of Airborne Bacteria in a Continuous-Flow Reactor. Ind. Eng. Chem. Res., 47, 7580-7585.

Shie, J.L., Lee, C.H., Chiou, C.S., Chang, C.T., Chang, C.C., Chang, C.Y. (2008) Photodegradation kinetics of formaldehyde using light sources of UVA, UVC and UVLED in the presence of composed silver titanium oxide photocatalyst. Journal of Hazardous Materials, 155, 164-172.

Shie, J.L., & Pai, C.Y. (2010) Indoor and Built Environment. Photodegradation Kinetics of Toluene in Indoor Air at Different Humidities Using UVA, UVC and UVLED Light Sources in the Presence of Silver Titanium Dioxide, 19(5), 503-512.

Subagio, D.P., Srinivasan, M., Lim, M., Lim, T.T. (2011) Photocatalytic degradation of bisphenol-A by nitrogen-doped TiO_2 hollow sphere in a vis-LED photoreactor. Applied Catalysis B: Environmental, 95(3-4), 414-422.

Vohra, A., Goswami, D.Y., Deshpande, D.A., Block, S.S. (2006) Enhanced photocatalytic disinfection of indoor air. Applied Catalysis B: Environmental, 64, 57-65.

WHO (2007) "Fact sheet N°104," World Health Organization.

Wang, W.Y. & Ku, Y. (2006) Photocatalytic degradation of Reactive Red 22 in aqueous solution by UV-LED radiation. Water Research 40, 2249-2258.

Yao, Y., Ochiai, T., Ishiguro, H., Nakano, R., Kubota, Y. (2011) Antibacterial performance of a novel photocatalytic-coated cordierite foam for use in air cleaners. Applied Catalysis B: Environmental, 106(3-4), 592-599.

Yu, K.-P., Lee, G.W.-M., Lin, S.-Y., Huang, C.P. (2008) Removal of bioaerosols by the combination of a photocatalytic filter and negative air ions. Journal of Aerosol Science, 39, 377-392.

Yu, H., Irie, H., Shimodaira, Y., Hosogi, Y., Kuroda, Y., Miyauchi, M., Hashimoto, K. (2010) An Efficient Visible-Light-Sensitive Fe(III)-Grafted TiO_2 Photocatalyst. The Journal of Physical Chemistry C, 114(39), 16481-16487.

Yuan, J., Hu, H., Chen, M., Shi, J., Shangguan, W. (2008) Promotion effect of Al_2O_3–SiO_2 interlayer and Pt loading on TiO_2/nickel-foam photocatalyst for degrading gaseous acetaldehyde. Catalysis Today, 139(1-2), 140-145.

Figure 1

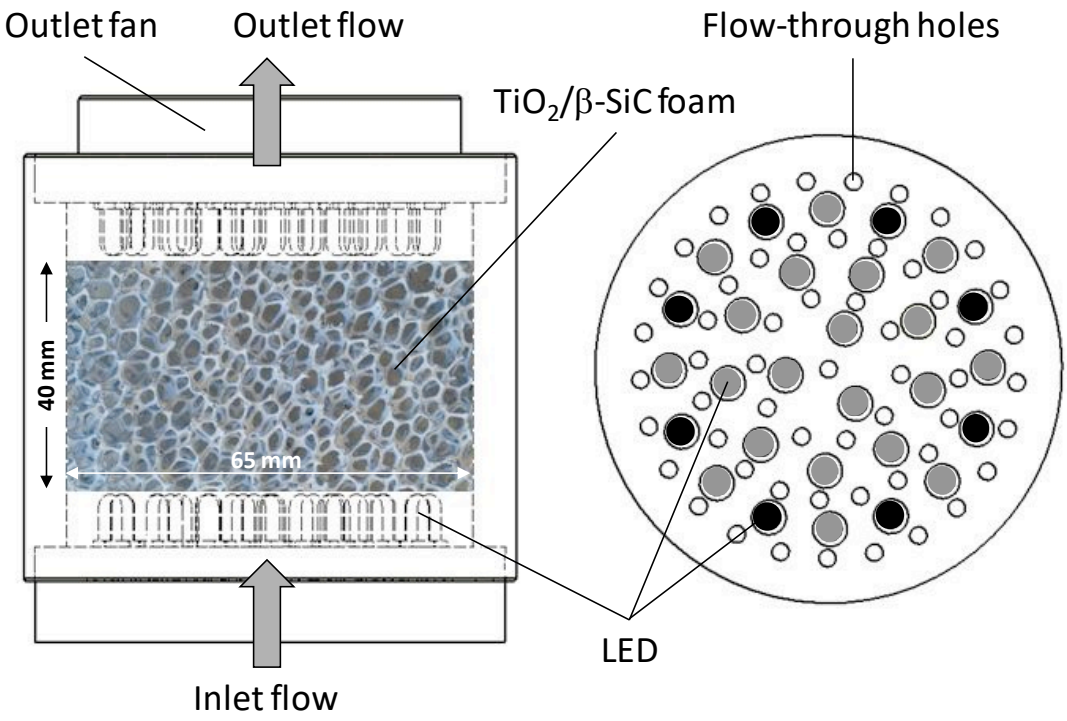

Scheme of the flow-through structured photocatalytic reactor incorporating LEDs and the TiO_2 MPT623/β-SiC foam. In addition to both top- and bottom-located LED printed circuit boards, it includes a 10 m^3/h inner fan for working in a recirculation mode inside the test chamber. In the 56 LED configuration, all the LEDs were lighted on (dark and grey), whereas only grey LEDs, were lighted on in the 40 LED configuration. The LEDs were equally distributed between both top- and bottom-printed circuits.

Figure 2

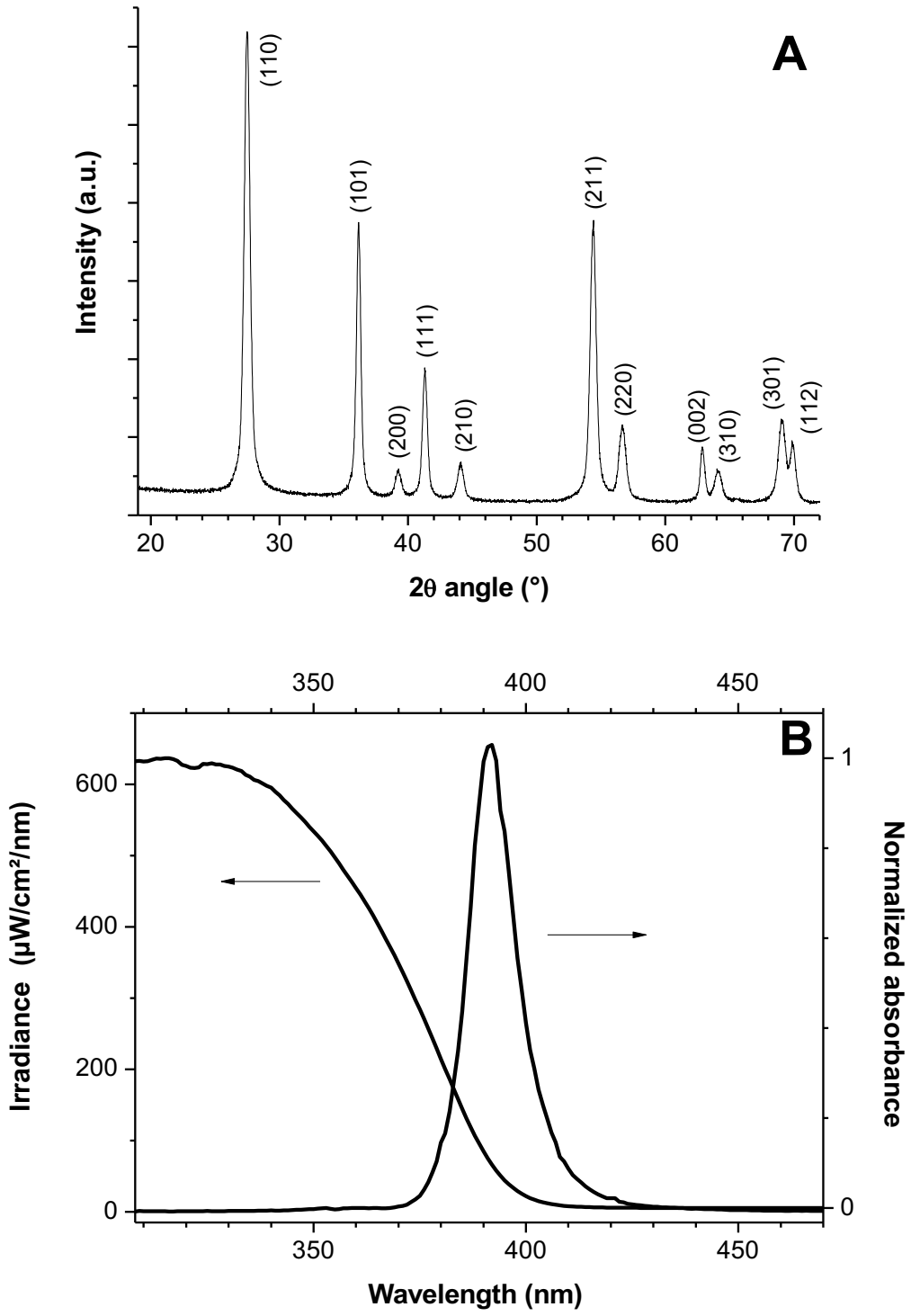

(A) XRD pattern of TiO_2 MPT623 ; **(B)** UV/vis absorption range of the commercially available TiO_2 MPT623 and LED-392 emission spectral range.

Figure 3

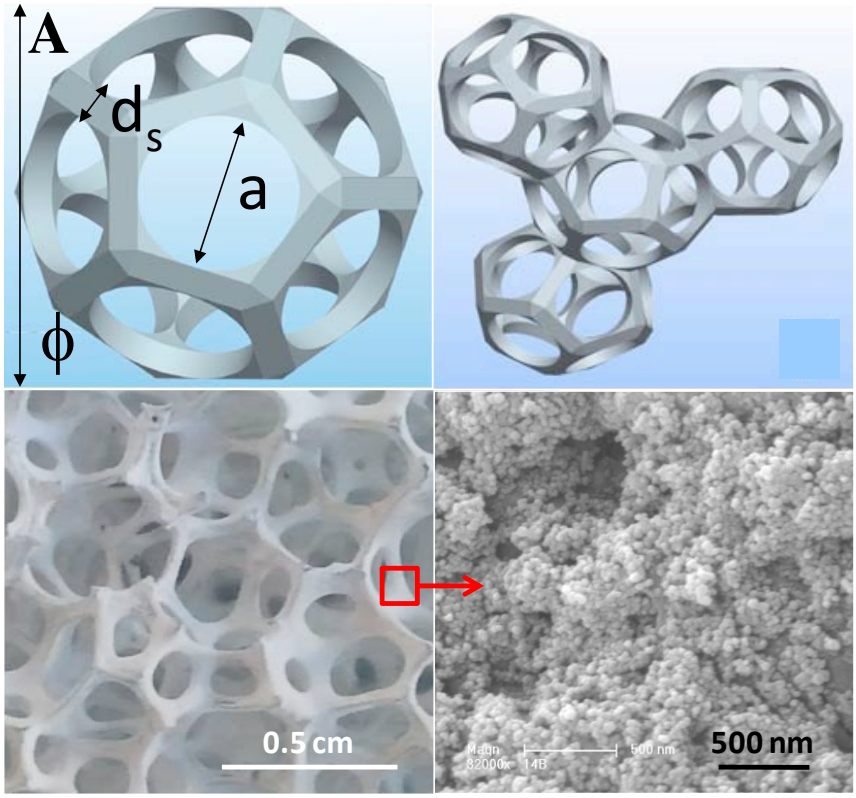

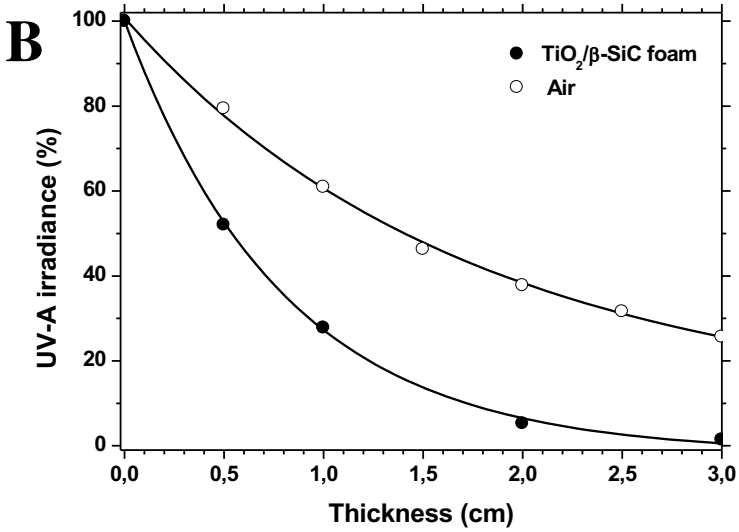

(A) *(top)* Schematic drawing of the model developed by Edouard, with packing of regular pentagonal dodecahedrons, taken from [45], visualizing the cell size (ϕ), the window size (a) and the strut diameter (ds) characteristics of the foam ;*(bottom)* Optical and SEM images of the open cell TiO_2 MPT623/β-SiC foam photocatalyst.

(B) UV-A light transmission within the TiO_2/β-SiC foam as a function of the foam thickness. The light transmission ability of the TiO_2/β-SiC foam, expressed as the foam characteristic length (λ) was derived from a $T_t = e^{-t/\lambda}$ first order decreasing exponential model as a function of the foam thickness *t*. Comparison with the natural decay of light irradiance in air.

Figure 4

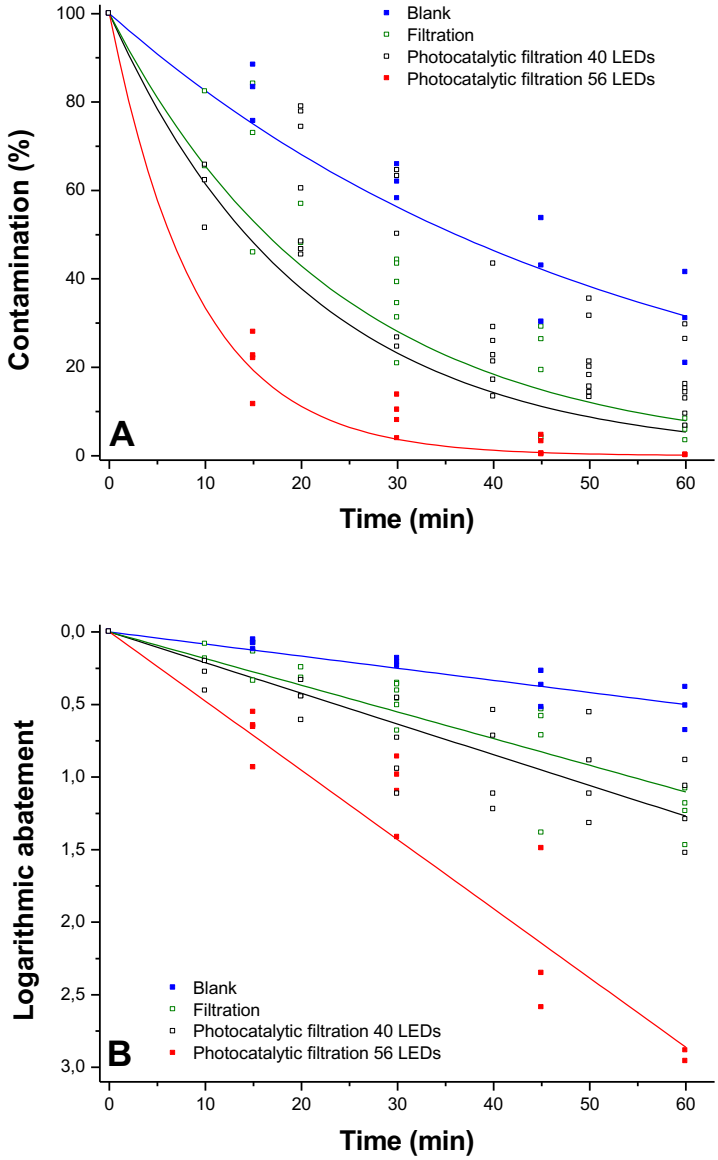

Decontamination kinetics of the bioaerosol of T2 bacteriophage viruses obtained with the 40 and 56 LEDs TiO_2/β-SiC foam structured photocatalytic reactors, expressed as the evolution with time on run of **(A)** the contamination and **(B)** the logarithmic abatement. The decontamination kinetic resulting from a pure filtration effect was reported irrespective of the number of LEDs, as well as blank test results, that represent the stability of the bioaerosol within the test chamber with time.

Photocatalytic filtration and filtration decontamination apparent time constants for the T2 bacteriophage virus bioaerosol obtained TiO_2/β-SiC foam structured photocatalytic reactors, with and without correction from the bioaerosol stability. The energy effectiveness (corrected or not from the bioaerosol stability) were calculated for 60 min of use, with an average value of 9.7 mW taken as input e considering the supplier data in the 8.1 mW (min) – 11.5 mW (max) range.

	Apparent time constant τ (min)	**Corrected apparent time constant τ_{corr} (min)**	**Energy effectiveness coefficient ($log.kW$**	
			Photocatalytic filtration	Photocatalytic fil (corrected for sta
t (min)	52.1	-		
t (min)	$\tau^{filtration} = 23.6$	$\tau^{filtration}{}_{corr} = 43.1$		
filtration with 40	$\tau^{photo} = 20.5$	$\tau^{photo}{}_{corr} = 33.8$	$4.5 \times 10^{+3}$	$3.2 \times 10^{+3}$
filtration with 56	$\tau^{photo} = 9.1$	$\tau^{photo}{}_{corr} = 11.0$	$5.5 \times 10^{+3}$	$4.6 \times 10^{+3}$